



Chinese Pharmaceutical Association
Institute of Materia Medica, Chinese Academy of Medical Sciences

Acta Pharmaceutica Sinica B

www.elsevier.com/locate/apsb
www.sciencedirect.com



ORIGINAL ARTICLE

The effect of lengths of branched-chain fatty alcohols on the efficacy and safety of docetaxel-prodrug nanoassemblies



Shuo Wang^{a,†}, Tian Liu^{a,†}, Yuetong Huang^a, Chaoying Du^a,
Danping Wang^b, Xiyan Wang^a, Qingzhi Lv^d, Zhonggui He^a,
Yinglei Zhai^{c,*}, Bingjun Sun^{a,*}, Jin Sun^{a,*}

^aWuya College of Innovation, Shenyang Pharmaceutical University, Shenyang 110016, China

^bSchool of Pharmacy, Shenyang Pharmaceutical University, Shenyang 110016, China

^cSchool of Medical Devices, Shenyang Pharmaceutical University, Shenyang 110016, China

^dSchool of Pharmacy, Binzhou Medical University, Binzhou 256600, China

Received 7 July 2023; received in revised form 18 August 2023; accepted 14 September 2023

KEY WORDS

Prodrugs;
Nanoassemblies;
Self-assembly;
Branched-chain fatty
alcohols;
Disulfide bond;
Docetaxel;
Efficacy;
Safety

Abstract The self-assembly prodrugs are usually consisted of drug modules, activation modules, and assembly modules. Keeping the balance between efficacy and safety by selecting suitable modules remains a challenge for developing prodrug nanoassemblies. This study designed four docetaxel (DTX) prodrugs using disulfide bonds as activation modules and different lengths of branched-chain fatty alcohols as assembly modules (C₁₆, C₁₈, C₂₀, and C₂₄). The lengths of the assembly modules determined the self-assembly ability of prodrugs and affected the activation modules' sensitivity. The extension of the carbon chains improved the prodrugs' self-assembly ability and pharmacokinetic behavior while reducing the cytotoxicity and increased cumulative toxicity. The use of C₂₀ can balance efficacy and safety. These results provide a great reference for the rational design of prodrug nanoassemblies.

© 2024 The Authors. Published by Elsevier B.V. on behalf of Chinese Pharmaceutical Association and Institute of Materia Medica, Chinese Academy of Medical Sciences. This is an open access article under the CC BY-NC-ND license (<http://creativecommons.org/licenses/by-nc-nd/4.0/>).

*Corresponding authors.

E-mail addresses: yingleizhai@aliyun.com (Yinglei Zhai), sunbingjun_spy@sina.com (Bingjun Sun), sunjin@syphu.edu.cn (Jin Sun).

[†]These authors made equal contributions to this work.

Peer review under the responsibility of Chinese Pharmaceutical Association and Institute of Materia Medica, Chinese Academy of Medical Sciences.

<https://doi.org/10.1016/j.apsb.2023.09.017>

2211-3835 © 2024 The Authors. Published by Elsevier B.V. on behalf of Chinese Pharmaceutical Association and Institute of Materia Medica, Chinese Academy of Medical Sciences. This is an open access article under the CC BY-NC-ND license (<http://creativecommons.org/licenses/by-nc-nd/4.0/>).

1. Introduction

Chemotherapy has a strong therapeutic effect in clinical practice but also brings serious adverse events^{1–6}. Many patients have to decrease the dose or discontinue treatment because of the intolerable toxic side effects^{7–9}. Therefore, reducing adverse events while ensuring the effect of chemotherapy has great research significance and clinical value^{10–13}. Nanotechnology offers a promising prospect for the targeted delivery of antiproliferative drugs^{14–16}. However, the delivery efficiency of traditional nano-drugs is often limited by the poor affinity between the carriers and the drugs, which leads to poor drug loading and potential carrier-related toxicity. There is an urgent need to develop more efficient and safe delivery strategies.

Carrier-free nanoassembly technology is expected to reduce chemotherapy toxicity through targeted delivery and avoid the safety risks caused by the use of carrier materials¹⁷. Carrier-free nanoassembly usually includes pure drug nanoassemblies, pro-drug nanoassemblies, and so on^{18–24}. Pure drug nanoassemblies refer to the self-assembly of only drugs, which is characterized by good safety without the use of carriers. However, this technology has relatively high requirements for drug structure, and most drugs need to be modified into prodrugs to achieve self-assembly. Compared to the traditional nanoparticles, the advantages of prodrug nanoassemblies are mainly reflected in two aspects: 1) The drug loading of prodrug nanoassemblies is higher (~50%) due to the prodrug nanoassemblies use the drug itself as the carrier; 2) The prodrug nanoassemblies use fewer carriers²⁵. The self-assembly prodrugs are usually consisted of three parts, including drug modules, activation modules, and assembly modules. At present, the common assembly modules are branched-chain and straight-chain fatty alcohols with “flexible” carbon chains^{12,26,27}. The prodrugs modified with branched-chain fatty alcohols have higher self-assembly ability than the prodrugs modified with straight-chain fatty alcohols due to the larger steric hindrance of branched-chain fatty alcohols. Therefore, the prodrug nanoassemblies with branched-chain fatty alcohols have better safety and pharmacokinetic behavior than those modified with straight-chain fatty alcohols²⁸. However, the risks of cumulative toxicity caused by the accumulation of drugs in normal tissues should not be ignored. Therefore, how to regulate the self-assembly stability of nanoassemblies to keep the balance between efficacy and safety is still a big challenge for the development of prodrug nanoassemblies.

In addition to the self-assembly stability²⁹, selective drug release at the tumor microenvironment is another key to building prodrug nanoassemblies with high efficiency and low toxicity. In contrast to normal cells, tumor cells exhibit a heterogeneous redox microenvironment due to the over-production of reactive oxygen species (ROS) and glutathione (GSH)^{30,31}. This phenomenon has been fully studied to trigger drug release in the tumor microenvironment. In our previous studies, we developed a series of prodrug nanoassemblies with sulfur or selenium bonds as activation modules^{28,29,31–33}. Among them, the α -disulfide bond exhibited redox dual-hypersensitivity, which was an ideal candidate for activation modules³⁰. Although redox hypersensitivity of the activation module can increase the antiproliferative activities, it would inevitably lead to premature drug release in blood circulation, thus causing systematic toxicity. Therefore, both the activation module and the assembly modules need to be precisely designed to achieve a precise balance between efficacy and safety.

In this study, four docetaxel (DTX) prodrugs were designed using α -disulfide bonds as activation modules, and different lengths of branched-chain fatty alcohols (2-hexyldecylalcohol, 2-heptylundecanol, 2-octyldodecylalcohol, or 2-decyltetradecyl alcohol) as assembly modules, correspondingly named as C₁₆-SS-DTX, C₁₈-SS-DTX, C₂₀-SS-DTX, and C₂₄-SS-DTX. The effects of carbon chain lengths on self-assembly stability, drug release behavior, cytotoxicity, pharmacokinetics, antineoplastic activity, and safety were systematically investigated. We found that the self-assembly stability and drug release ability of the prodrug nanoassemblies were affected by changing the lengths of the branched-chain fatty alcohols. Among them, C₂₀-SS-DTX, with high self-assembly stability and high redox sensitivity, ensured a good balance between efficacy and safety. This research will provide a reference significance for the rational design of prodrug nanoassemblies.

2. Materials and methods

2.1. Materials

Docetaxel (DTX), trypsin, glutathione (GSH), and thiazolyl blue (MTT) were all provided by Meilun Biotechnology (Dalian, China). *N*-(Carbonyl-methoxy polyethylene glycol 2000)-1,2-distearoyl-*sn*-glycerol-3-phosphoethanolamine (DSPE-mPEG_{2K}) was derived from AVT (Shanghai) Pharmaceutical Tech Co., Ltd. (Shanghai, China). Thioglycolate disulfide, 2-hexyldecylalcohol, 2-heptylundecanol, 2-octyldodecylalcohol, 2-decyltetradecyl alcohol, coumarin-6 (C-6), *N*-(3-dimethylaminopropyl)-*N'*-ethyl carbodiimide hydrochloride (EDCI), hydrogen peroxide (H₂O₂), 4-dimethylaminopyridine (DMAP), and 1-hydroxybenzotriazole anhydrous (HOBT) were acquired by Shanghai Aladdin Biochemical Technology Co., Ltd. (Shanghai, China). Microtubule Tracker Red detection kit was purchased from Baiaolaibo Technology Co., Ltd. (Beijing, China). Annexin V-FITC/PI apoptosis detection kit came from Beijing Solarbio Science & Technology Co., Ltd. (Beijing, China). Cell culture medium, plates, and dishes were obtained by NEST Biotechnology Co., Ltd. (Wuxi, China). All other reagents used in this paper were of analytical or high-performance liquid chromatography (HPLC) grade.

2.2. Synthesis of prodrugs

Acetic anhydride (10 mL) reacted with dithiodiacetic acid (8 mmol) under nitrogen atmosphere (N₂) at 25 °C for 2 h. Then the product above without acetic anhydride was applied to dissolve in a round bottom immediately with dichloromethane (30 mL). The solution of DMAP (0.8 mmol) and the solution of 2-hexyldecylalcohol, 2-heptylundecanol, 2-octyldodecylalcohol, or 2-decyltetradecyl alcohol (4 mmol) were added to the reaction system drop by drop. Then the reaction was under N₂ for 12 h. After purification, the organic solvent was removed, and the products (C₁₆/C₁₈/C₂₀/C₂₄-SS) were obtained.

The products (C₁₆/C₁₈/C₂₀/C₂₄-SS) (0.3 mmol) were dissolved with dichloromethane. The catalysts including EDCI (0.6 mmol), DMAP (0.12 mmol), and HOBT (0.3 mmol) were dissolved with the solvent above, and then the solution was mixed with the reaction system and activated at 0 °C under the protection of N₂. The DTX (0.25 mmol) was added to the reaction system above at 25 °C for 36 h. The final product was separated by preparative

liquid chromatography. The structures of prodrugs were confirmed by ^1H NMR spectroscopy and HRMS. The purity of the four prodrugs was determined by the reverse-phase HPLC system.

2.3. Preparation and characterization of DTX prodrugs nanoassemblies (DPNAs)

The DPNAs were prepared by the one-step nano-precipitation method. For PEGylated DPNAs, the prodrugs and DSPE-mPEG_{2K} ($w/w = 20\%$) were dissolved in ethanol. The mixture was slowly added into deionized water under stirring conditions (1000 r/min). Then the ethanol was removed from the DPNAs using the rotary evaporator at 30 °C. Particle sizes and zeta potential of the DPNAs were measured by the Zetasizer (Malvern Co., UK). The morphologies of the DPNAs were examined by TEM. The non-PEGylated DPNAs^{18,19} and the C-6 labeled DPNAs were prepared by the same method.

2.4. Colloidal stability

The particle sizes of the DPNAs were used as the standard to study the effect of the lengths of assembly modules on the self-assembly stability of DPNAs. The DPNAs were incubated in the medium [phosphate-buffered saline (PBS, pH 7.4) containing 10% fetal bovine serum (FBS)] in the constant temperature oscillator at 37 °C. The particle sizes of the DPNAs were measured at the indicated time using Zetasizer (Malvern). At the same time, the stability of PEGylated DPNAs was evaluated after being stored at 4 °C for 70 days.

2.5. Redox dual-sensitive drug release

The release behavior of DPNAs was studied *in vitro*. The four DPNAs (0.2 mL, 1 mg/mL) were respectively diffused in release medium ($n = 3$) (volume = 30 mL) containing H₂O₂ (1 mmol/L, 10 mmol/L) or GSH (0.05 mmol/L, 1 mmol/L), and incubated at 37 °C. The concentration of the DTX released was determined by HPLC.

2.6. Cell uptake

Mouse mammary tumor cells (4T1 cells) with culturing on cell slides for 24 h were incubated with the C-6 solution or C-6 labeled DPNAs (250 ng/mL, equivalent to free C-6) for 0.5 or 2 h at 37 °C. After that, cells were washed with PBS (4 °C) to terminate cell uptake. Then, 4% paraformaldehyde was added to hold the cells for 10 min and carefully washed as before. The nuclei were stained with Hoechst 33342. Finally, the confocal laser scanning microscope (CLSM, C2SI, Nikon, Japan) was used to observe the images of cells.

2.7. Cytotoxicity assay

MTT assay was used to assess the antiproliferative activities of Taxotere or DPNAs against 4T1 cells, mouse melanoma cells (B16–F10 cells), human oral epidermoid carcinoma cell line (KB cells), human pulmonary epithelial cell (A549 cells), mouse embryonic fibroblast cell line (3T3 cells), and human normal liver cells (L02 cells). All kinds of cells were respectively cultured for 24 h, and the medium containing Taxotere or DPNAs was replaced with the blank medium for 48 h. Then the cells were treated with MTT. After 4 h, the purple formazan crystals were dissolved in

dimethyl sulfoxide (DMSO). The enzyme-labeled instrument (SYNERGY, BioTek Instruments, Inc, USA) was used to measure the absorbance at 490 nm. The IC₅₀ was calculated using GraphPad Prism 8.0. The tumor-selective index (SI) was calculated as Eq. (1):

$$SI = IC_{50\text{normal}} / IC_{50\text{tumor}} \quad (1)$$

where IC_{50normal} and IC_{50tumor} represent the IC₅₀ of Taxotere or DPNAs toward normal cells and tumor cells.

2.8. Cell apoptosis assay

After 4T1 cells were cultured for 24 h, the blank medium was replaced with a medium containing the Taxotere or DPNAs (500 nmol/L) and incubated cells for 24 h. The cells were washed with PBS (4 °C), digested, collected, and centrifuged. Then the cells were processed according to the procedure recommended by the Annexin V-FITC/PI apoptosis detection kit (Solarbio). Finally, the results of cell apoptosis were measured by flow cytometer (Becton Dickinson, USA), and the results were analyzed using FlowJo software.

2.9. Tubulin inhibition assay

After 4T1 cells were cultured on cell slides for 24 h, medium containing Taxotere and DPNAs (100 nmol/L) were respectively added to the plates and incubated for 48 h. Then the cells were processed according to the procedure recommended by the Microtubule Tracker Red detection kit (Baiolabo). Finally, CLSM (C2SI, Nikon) was used to observe the images of cells.

2.10. Intracellular drug release

The relationship between the intracellular behavior of drug release and the lengths of assembly modules was explored. 4T1 cells (10⁵ cells per well) were cultured for 24 h. The cells were incubated with the medium containing the Taxotere or DPNAs (200 ng/mL, 500 ng/mL) for 48 h. The cell culture medium and cells were collected into the corresponding centrifuge tubes, after which the cells were destroyed by ultrasound and centrifugation. Finally, the quantitative volume was extracted from the supernatant, and the concentrations of DTX released were analyzed by the UPLC–MS–MS system (Xevo TQ, Waters, USA).

2.11. Animal studies

All the animal experiments were performed by the Guide for the Management and Use of Laboratory Animals and were approved by the Institutional Animal Ethical Care Committee (IAEC) of Shenyang Pharmaceutical University.

2.12. Pharmacokinetic study of DPNAs *in vivo*

The pharmacokinetic behavior of Taxotere and DPNAs was investigated. Sprague–Dawley (SD) rats fasting for 12 h were randomly split into 5 groups ($n = 5$). Then the SD rats were injected intravenously with Taxotere or DPNAs at the dose of 4 mg/kg (equivalent to DTX). Blood was respectively collected, and plasma was separated from the posterior ocular venous cluster of rats at the indicated time (0.033, 0.083, 0.25, 0.50, 1, 2, 4, 8, 12, and 24 h). The protein in the plasma was removed by the protein

precipitation method. Paclitaxel (PTX) was used as the internal standard. Finally, the plasma concentrations of prodrugs or free DTX was determined by the UPLC–MS–MS system (Xevo TQ, Waters).

2.13. *In vivo antineoplastic activity*

The 4T1 mouse transplanted tumor model was established by inserting tumor cells into the BALB/c mice. Taxotere or DPNA were injected intravenously in mice at a dose of 2.5 mg/kg (equivalent to DTX, $n = 5$) when the tumor volume was measured to be about 100 mm³. Normal saline was injected as a blank control group. The preparation was administered once every two days through the caudal vein for a total of five injections. The tumor volume and body weight of all mice were recorded every day. Among them, the tumor volume was calculated as Eq. (2):

$$\text{Tumor volume (mm}^3\text{)} = (\text{Length} \times \text{Width}^2)/2 \quad (2)$$

One day after the fifth treatment, all mice were executed. Then isolated tumors were imaged, grouped, and weighed. The tumor burden was calculated as Eq. (3):

$$\text{Tumor burden} = \text{Tumor weight} / \text{Body weight} \quad (3)$$

The serum and whole blood were collected for assessment of hepatorenal function analysis and blood routine.

The A549 nude-mouse transplanted tumor model was established by inserting tumor cells into immunodeficient nude mice. Taxotere or DPNA (C₁₈-SS-DTX NPs, C₂₀-SS-DTX NPs) were injected intravenously in mice at a dose of 20 mg/kg (equivalent to DTX, $n = 3$) when the tumor volume was measured to be about 170 mm³. Normal saline was injected as a blank control group. The preparation was administered through the tail vein at the indicated time (Days 0, 4, and 7) for a total of three injections. The data of all mice were recorded every day. On day 17, all mice were sacrificed, and then isolated tumors were imaged, grouped, and weighed. The tumor volume and tumor burden were calculated as before.

2.14. *The study of acute toxicity*

Taxotere and DPNA were respectively injected in healthy female BALB/c mice at a dose of 10 and 100 mg/kg (equivalent to DTX, $n = 3$). Because of the tolerated volume of a single intravenous injection in mice and the good safety of the DPNA, the preset dose could not be achieved by a single intravenous injection. Therefore, we used the cumulative dosing method: DPNA were injected at a dose of 100 mg/kg every 15 min to characterize the acute toxicity test (equivalent to DTX). When the cumulative dosage reached 500 mg/kg, the subsequent administration time was set as once every 4 h to avoid sudden death caused by the excessive volume of administration, with a total of seven injections. The body weight and survival status of mice were recorded.

2.15. *Cumulative toxicity study*

The tolerated volume of DPNA was explored using healthy female BALB/c mice. Mice were intravenously given Taxotere or DPNA (C₁₈-SS-DTX NPs, C₂₀-SS-DTX NPs) at the dose of

30 or 45 mg/kg (equivalent to DTX, $n = 6$). The Taxotere and DPNA (C₂₀-SS-DTX NPs, C₂₄-SS-DTX NPs) were respectively administered through the tail vein every 4 days. The survival and body weight of each group of mice were recorded daily for 11 days.

2.16. *Statistical analysis*

Data were calculated as mean value \pm standard deviation (SD). Statistical differences between the two groups were analyzed by Student's *t*-test (two-tailed) and one-way (ANOVA). Statistical significance was recorded at n.s.: $P > 0.05$ (no significance), * $P < 0.05$, ** $P < 0.01$, *** $P < 0.001$, and **** $P < 0.0001$.

3. Results and discussion

3.1. *Synthesis of prodrugs*

Four redox dual-sensitive prodrugs were designed and synthesized using disulfide bonds as activation modules, connected with 2-hexyldecylalcohol, 2-heptylundecanol, 2-octyldodecylalcohol, or 2-decyltetradecyl alcohol, respectively. Accordingly, the above four prodrugs were named C₁₆-SS-DTX, C₁₈-SS-DTX, C₂₀-SS-DTX, and C₂₄-SS-DTX, respectively. The synthetic pathways were illustrated in Supporting Information Fig. S1. And the chemical structures of four prodrugs were determined by ¹H NMR and HRMS (Supporting Information Figs. S2–S5). The NMR results were analyzed: the NMR hydrogen spectra contained characteristic peaks of docetaxel ring structure in the range of 7–8 ppm and branched fatty alcohols in the range of 1–2 ppm. At the same time, the sodium peaks of the prodrugs were detected by HRMS. All the above results proved the synthesis of the prodrugs. Furthermore, the purity of the four prodrugs exceeded 99% (Figs. S2–S5), which met the demands of follow-up experiments.

3.2. *Preparation and characterization of DPNA*

In this study, we investigated the self-assembly ability of DPNA with different lengths of branched-chain fatty alcohols. Firstly, the DPNA without surfactant modification were prepared by the one-step nano-precipitation method, which were named as non-PEGylated C₁₆-SS-DTX NPs, non-PEGylated C₁₈-SS-DTX NPs, non-PEGylated C₂₀-SS-DTX NPs, and non-PEGylated C₂₄-SS-DTX NPs, respectively. Then, we studied their self-assembly ability. At the concentration of 0.05 mg/mL, the C₁₈-SS-DTX, C₂₀-SS-DTX, and C₂₄-SS-DTX could spontaneously assemble into nanoassemblies (Supporting Information Fig. S6A) with a count rate of about 150, and the particle sizes of the three DPNA were 640.60, 236.70, and 202.80 nm (Supporting Information Table S1), respectively. However, the count rate of non-PEGylated C₁₆-SS-DTX NPs was only about 30 (Supporting Information Table S2), indicating that the C₁₆-SS-DTX failed to assemble into nanoassemblies. We analyzed that this may be due to the weak hydrophobicity of C₁₆-SS-DTX, which leads to the insufficient driving force to form the nanoassemblies. With the concentrations of preparation increased to 0.08 mg/mL (Fig. S6B) and 0.1 mg/mL (Fig. S6C), the particle sizes of non-PEGylated C₂₄-SS-DTX NPs were 193.20 and 201.80 nm. In comparison, significant precipitation was found in non-PEGylated C₁₈-SS-DTX NPs and non-PEGylated C₂₀-SS-DTX NPs at the same

concentration, and C₁₆-SS-DTX still couldn't assemble into nanoassemblies. In conclusion, the order of self-assembly ability of four prodrugs was C₂₄-SS-DTX > C₂₀-SS-DTX > C₁₈-SS-DTX > C₁₆-SS-DTX.

We further investigated the reasons for the differences in the self-assembly ability of the four DPNA. The key factors affecting molecular self-assembly were aggregation driving force and structural flexibility. The only difference between the four DPNA was the lengths of assembly modules, which provided a strong hydrophobic force for self-assembly. Therefore, we calculated the oil-water partition coefficient ($\log P$) of the four prodrugs by MarvinSketch to judge their hydrophilicity and hydrophobicity. As shown in Supporting Information Fig. S7, the $\log P$ values of C₁₆-SS-DTX, C₁₈-SS-DTX, C₂₀-SS-DTX, C₂₄-SS-DTX, and DTX respectively were 10.46, 11.35, 12.24, 14.01 and 2.92. It proved that prodrugs were provided with higher hydrophobicity through the longer carbon chains of assembly modules. Thus C₂₄-SS-DTX had the highest driving force for the self-assembly due to the

highest hydrophobicity. In addition, the number of σ bonds increased with the extension of the carbon chains, and thereby more flexible molecular structure facilitated the adjustment of the prodrugs to the lowest energy state in the self-assembly process (Supporting Information Fig. S8). The results showed that the different lengths of branched-chain fatty alcohols of prodrugs could significantly affect the self-assembly ability and that with the extension of the carbon chains, the self-assembly ability of the prodrugs was improved (Fig. 1).

To prolong the circulation time of DPNA *in vivo*, DSPE-mPEG_{2K} was modified onto the surface of the DPNA. The PEGylated DPNA were prepared and named C₁₆-SS-DTX NPs, C₁₈-SS-DTX NPs, C₂₀-SS-DTX NPs, and C₂₄-SS-DTX NPs, respectively. The particle sizes of the PEGylated DPNA were about 80 nm (Fig. 2B), the zeta potential of DPNA was about -30 mV, and the drug loading was about 45%–55% (Supporting Information Table S3). The prepared PEGylated DPNA were uniformly spherical (Fig. 2C) and were found to be stable at 4 °C

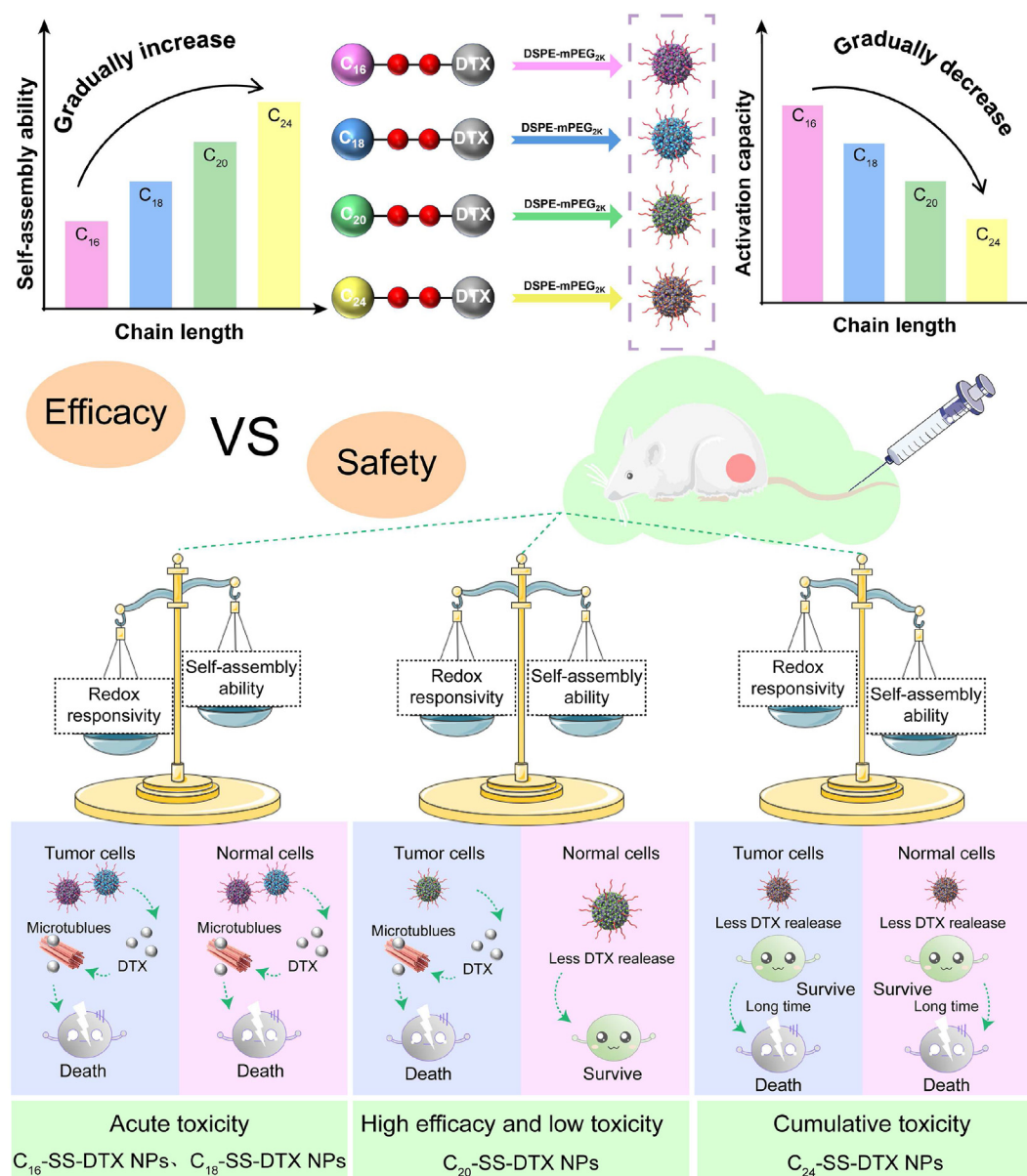


Figure 1 Schematic diagram of DTX prodrugs nanoassemblies with different assembly modules for efficient chemotherapy.

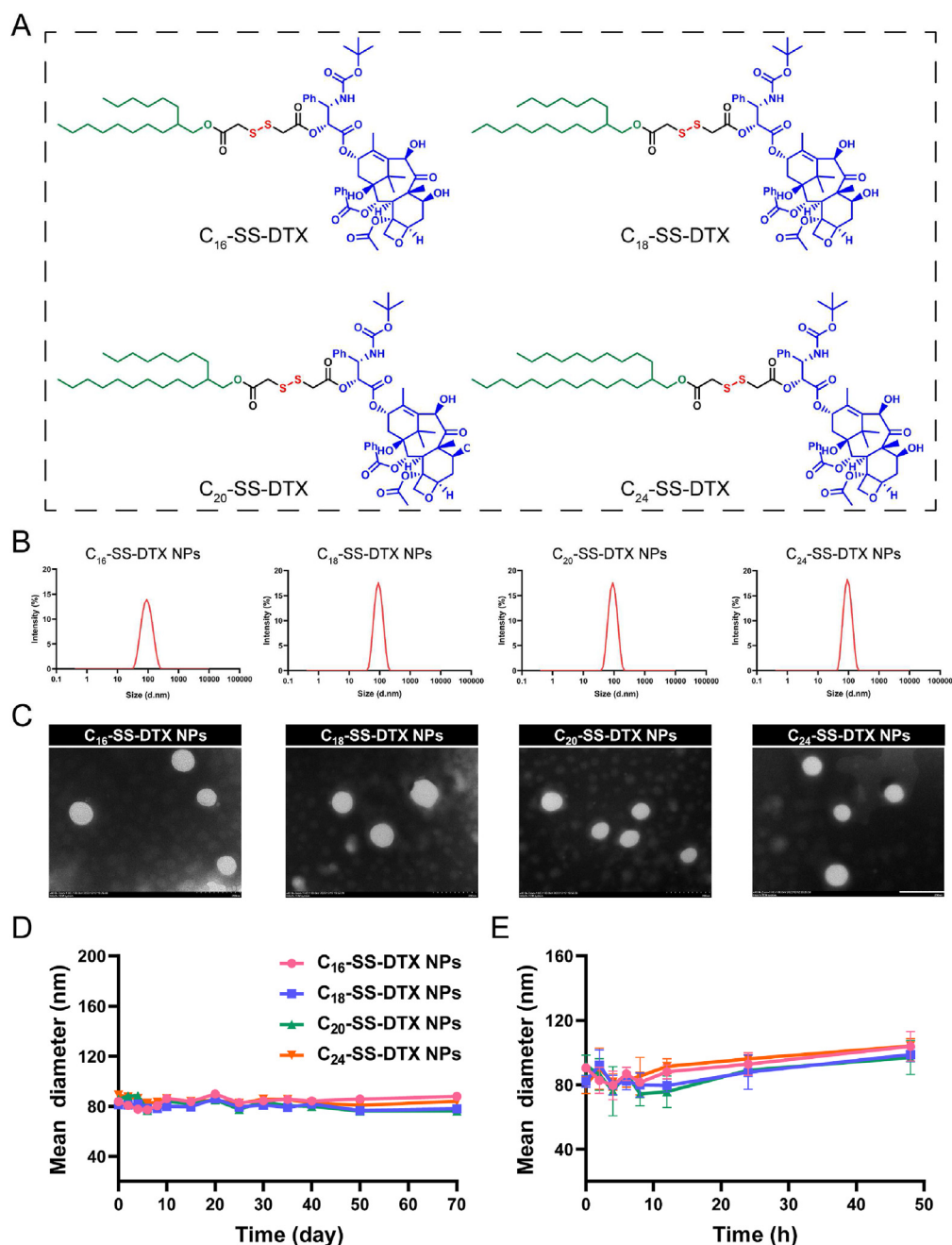


Figure 2 Preparation and characterization of DPNA. (A) Chemical structures of four prodrugs. (B) Particle sizes of DPNA. (C) Morphology of DPNA obtained by transmission electron microscopy (TEM, Hitachi, Japan). Scale bar represents 200 nm. (D) Storage stability of DPNA at 4 °C. (E) The changes of particle size of DPNA after co-incubation with FBS-containing PBS for 48 h. Data are presented as mean \pm SD ($n = 3$).

for 70 days (Fig. 2D). In addition, PEGylated DPNA remained stable for 48 h after dilution with PBS (pH 7.4) with FBS ($v/v = 10\%$, Fig. 2E). These results indicated that DSPE-mPEG_{2K} could improve the stability of DPNA, so PEGylated DPNA was selected for subsequent experiments.

3.3. Redox dual-sensitive drug release

The release of DTX from DPNA was particularly important for their antiproliferative activity and safety. Only a small amount of DTX (<5%) was released from DPNA within 24 h in the blank

medium (PBS with 30% ethanol) without H₂O₂ and GSH. DTX was rarely released in a non-redox environment, which means that DPNA will not leak in normal tissues in advance, thus avoiding toxic and side effects caused by excessive DTX exposure (Supporting Information Fig. S9). Then we used H₂O₂ (the main component of ROS *in vivo*) and GSH as redox agents to study the drug release of DPNA in the redox conditions. The results confirmed that DPNA showed redox dual-triggered drug release (Fig. 3A–D).

The release rate of DPNA under oxidation conditions was: C₁₆-SS-DTX NPs > C₁₈-SS-DTX NPs > C₂₀-SS-DTX

NPs > C₂₄-SS-DTX NPs. We analyze that the difference in this result comes from the oxidation-responsive mechanism of the disulfide bond (Fig. 3E) elucidated in our previous work¹³: sulfur atoms were oxidized by H₂O₂ to generate hydrophilic sulfoxide or sulphone, which facilitated the release of DTX. In prodrugs, hydrophobic groups could shield disulfide bonds. Therefore, the larger the hydrophobic group, the more difficult it was for hydrogen peroxide to attack disulfide bonds. The release rate of C₂₄-SS-DTX was the slowest under oxidation conditions due to

the highest hydrophobicity, which was not conducive to ester bond hydrolysis.

However, we found the release rates of DPNAs were similar under the same reduction condition. The reduction-responsive mechanism of the disulfide bond was shown in Fig. 3F. The mercaptan intermediate (DTX-SH) was generated since the disulfide bond was attacked by GSH. As the four DPNA s had the same intermediates, the structure of assembly modules had a negligible effect on the reduced sensitivity of the DPNA s.

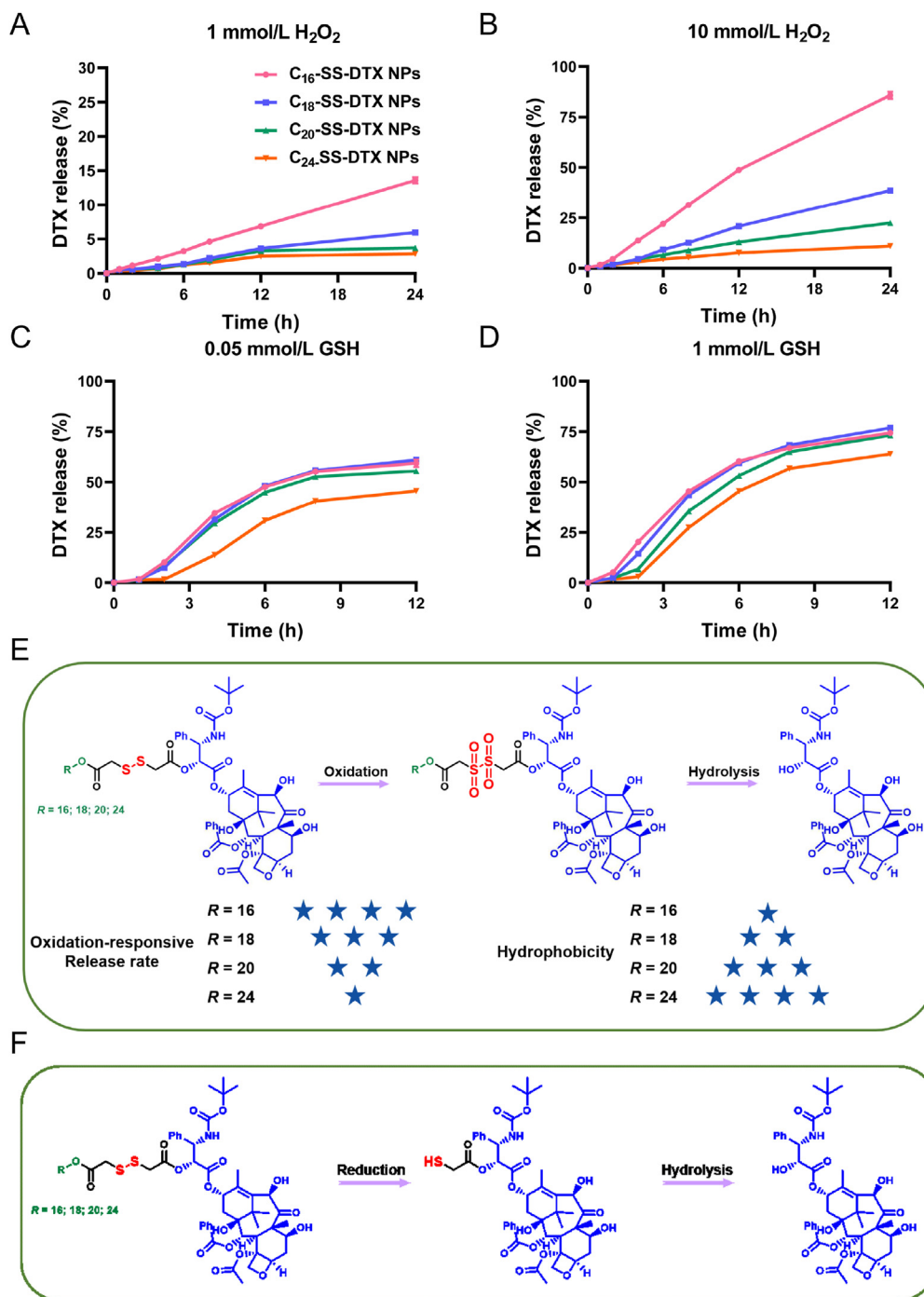


Figure 3 Redox dual-sensitive drug release. (A) 1 mmol/L H₂O₂; (B) 10 mmol/L H₂O₂; (C) 0.05 mmol/L GSH; (D) 1 mmol/L GSH. The oxidation mechanism (E) and the reduction mechanism (F) of DPNA s. Data are presented as mean ± SD (*n* = 3).

3.4. Cytological study

Cellular uptake is the key step in the bioactivation of DPNA. The intracellular fluorescence intensity was detected by CLSM (C2SI, Nikon). As shown in Supporting Information Fig. S10, cells treated with coumarin-6 (C-6) labeled DPNA showed significantly higher intracellular fluorescence intensity compared with the free C-6. Furthermore, the four DPNA exhibited comparable cellular uptake due to their similar surface properties in terms of particle size (~ 80 nm) and zeta potential (~ -30 mV).

The cytotoxicity of DPNA was studied in 4T1 cells, B16–F10 cells, KB cells, A549 cells, 3T3 cells, and L02 cells. The results were summarized in Fig. 4A–F, Supporting Information Fig. S11A–S11F and Supporting Information

Table S4. Because of the drug release process, DPNA showed lower cytotoxicity than Taxotere in the order of Taxotere > C₁₆-SS-DTX NPs > C₁₈-SS-DTX NPs > C₂₀-SS-DTX NPs > C₂₄-SS-DTX NPs. Since the four DPNA showed similar cellular uptake, it was suggested the difference in cytotoxicity may be related to the release rate of DTX. The results of the intracellular release of DTX from DPNA were consistent with the results of cytotoxicity (Fig. 4G and H). It was proved that the shorter the lengths of carbon chains, the higher the release rate of DTX and the higher the cytotoxicity.

In addition, we found that the toxicity of the DPNA to normal cells was significantly reduced, and DPNA showed a higher selectivity index (SI) in tumor cells compared with Taxotere (Supporting Information Tables S5 and S6). This was due to

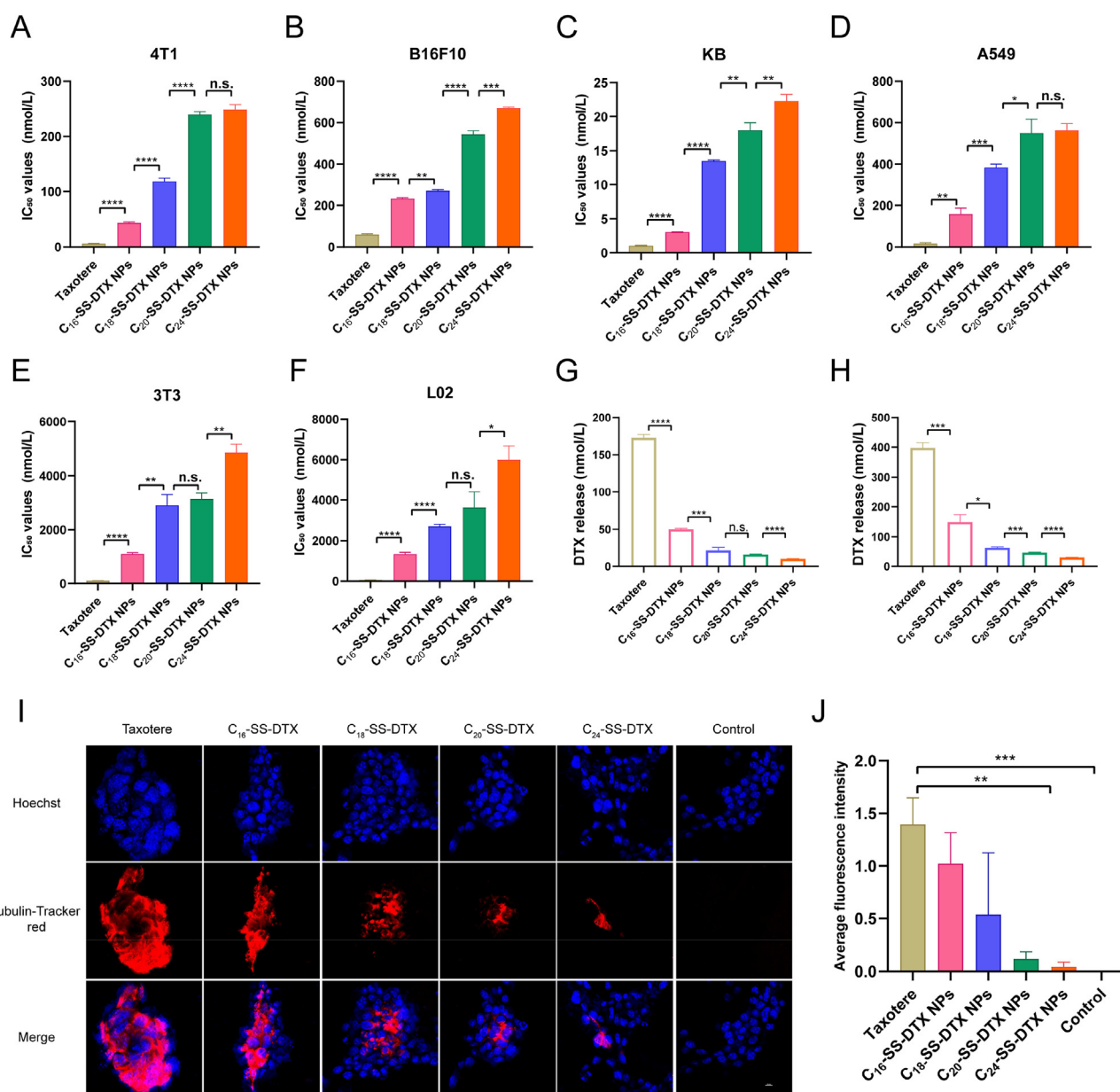


Figure 4 Cytological study. (A–F) IC₅₀ values of Taxotere and DPNA in 4T1 cells, B16–F10 cells, KB cells, A549 cells, 3T3 cells, and L02 cells. Free DTX released from DPNA (200 ng/mL) (G) and (500 ng/mL) (H) after incubation with 4T1 cells for 48 h. (I) Inhibitory effect of Taxotere and DPNA on tubulin. Scale bar represents 10 μ m. (J) Fluorescence quantitative results of CLSM images. Data are presented as mean \pm SD ($n = 3$). n.s. (no significance) $P > 0.05$, * $P < 0.05$, ** $P < 0.01$, *** $P < 0.001$, and **** $P < 0.0001$ by two-tailed Student's t -test.

higher ROS levels in tumor cells (4T1 cells, B16–F10 cells, KB cells, and A549 cells) than in normal cells (3T3 cells and L02 cells) (Fig. S11G and I). This demonstrated that DPNA with intelligent activation modules could be specifically activated in the tumor microenvironment, which is expected to provide a safer antiproliferative therapy.

The microtubule red fluorescent probe could mark microtubules in the aggregated state and verify the inhibitory effect of the drugs on the depolymerization of tubulin. As shown in Fig. 4I and J, the Taxotere had the highest inhibitory effect on tubulin depolymerization, followed by C₁₆-SS-DTX NPs, C₁₈-SS-DTX NPs, C₂₀-SS-DTX NPs, and C₂₄-SS-DTX NPs. In addition, the apoptosis rates of cells after being treated with Taxotere and DPNA were as follows: Taxotere (57.2%), C₁₆-SS-DTX NPs (41.0%), C₁₈-SS-DTX NPs (36.9%), C₂₀-SS-DTX NPs (31.5%) and C₂₄-SS-DTX NPs (21.2%, Supporting Information Fig. S12). The above results could be correlated with the results of cytotoxicity, which indicated that the intracellular release rate of DTX was positively correlated with the inhibition of tubulin and the degree of apoptosis. In conclusion, C₁₆-SS-DTX NPs had the strongest cytotoxicity due to the highest release rate of active DTX.

3.5. Pharmacokinetic of DPNA in vivo

The pharmacokinetic behavior of DPNA was affected by self-assembly stability and redox dual-sensitivity. DPNA are expected to have high self-assembly stability and low redox sensitivity to ensure the long circulation of DPNA in vivo. For ease of comparison, the pharmacokinetic profiles were shown in Fig. 5A–C, and the pharmacokinetic parameters were summarized in

Supporting Information Table S7. It can be seen that the proportion of parent drugs released by prodrug nanoassemblies is small in systemic circulation through the pharmacokinetic parameters. This proved that prodrug nanoassemblies can have good stability in the systemic circulation. The higher area under the curve (AUC) values (the sum of prodrugs and parent drugs) of C₁₆-SS-DTX NPs, C₁₈-SS-DTX NPs, C₂₀-SS-DTX NPs, and C₂₄-SS-DTX NPs were 85.44, 100.44, 107.81 and 112.09 times of Taxotere, respectively. Compared with Taxotere, DPNA have a higher AUC, longer half-lives, and lower plasma clearance (CL), which is conducive to improving tumor accumulation. At the same time, prodrug nanoassemblies can be effectively activated in tumor cells to ensure antineoplastic activity according to cytotoxicity and intracellular drug release.

As the above results showed, the C₂₄-SS-DTX NPs showed the highest AUC value due to good self-assembly stability, followed by C₂₀-SS-DTX NPs, C₁₈-SS-DTX NPs, and C₁₆-SS-DTX NPs. Compared with reductive sensitivity, oxidative sensitivity played the dominant role in affecting the pharmacokinetic behavior of DPNA due to the high level of oxygen in the blood. Among the DPNA, C₁₆-SS-DTX NPs had the highest oxidation sensitivity and the highest release rate of DTX, resulting in the short blood-circulation pharmacokinetic behavior of C₁₆-SS-DTX NPs. In summary, the lengths of the assembly modules had a significant influence on the pharmacokinetic behavior, and the longer the lengths of the carbon chains, the higher the self-assembly stability, the lower the oxidation sensitivity, and the better the pharmacokinetic behavior. Therefore, C₂₀-SS-DTX NPs and C₂₄-SS-DTX NPs exhibited better pharmacokinetic behavior due to their better self-assembly stability and lower oxidation sensitivity.

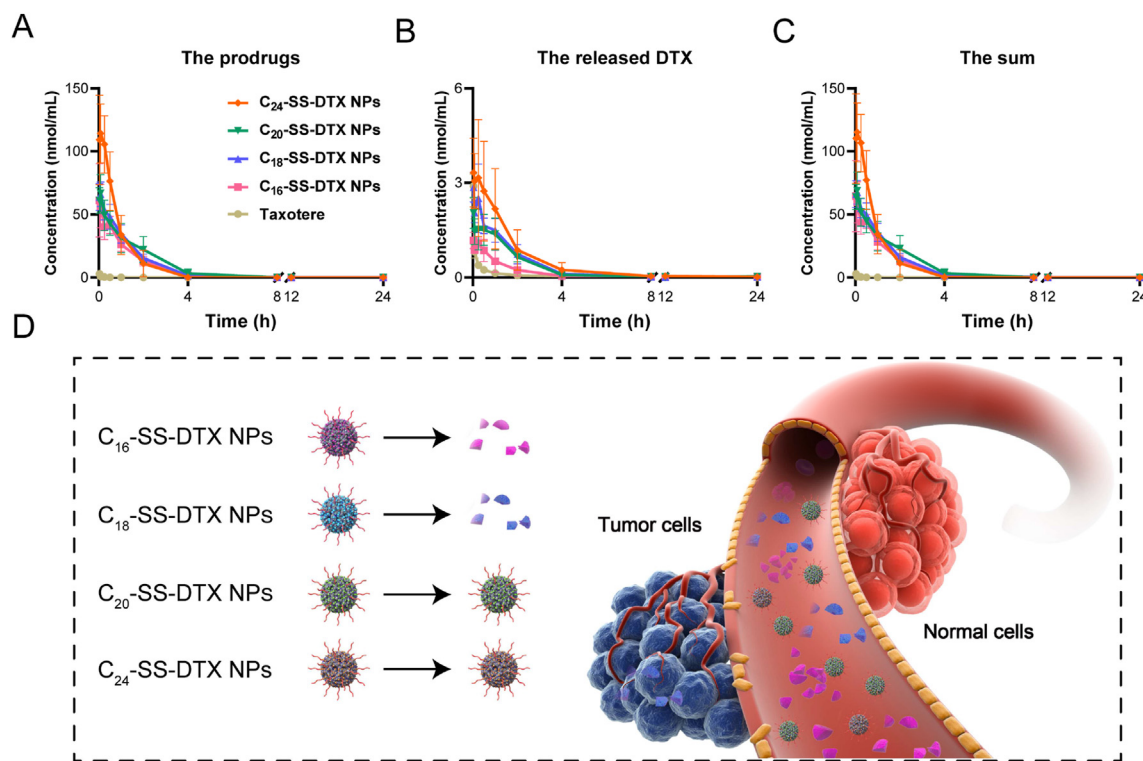


Figure 5 Pharmacokinetics of DPNA. Pharmacokinetic profiles of the (A) prodrugs, (B) released DTX, and (C) total equivalent DTX. (D) Schematic of pharmacokinetic. Data are presented as mean \pm SD ($n = 5$).

3.6. Antineoplastic activity and safety of DPNAs in vivo

Firstly, we established a 4T1 tumor model to study the effect of assembly modules on the antineoplastic activity of DPNAs at a low dose (2.5 mg/kg). As shown in Fig. 6B–D and Supporting Information Fig. S13, DPNAs exhibited stronger antineoplastic activity in the tumor volume and tumor burden than Taxotere. There was no significant difference in antineoplastic activity between the four DPNAs. In terms of safety, body weight and monocyte count (Mon) (Supporting Information Fig. S14) were significantly reduced in mice treated with Taxotere compared to the saline, suggesting that Taxotere had caused serious toxicity. In comparison, there were no significant changes in body weight, blood routine, or hepatic and renal function analysis of the four DPNAs compared with the saline. These results indicated that DPNAs had potent antineoplastic activity and good safety. At the

same time, there was no significant difference in antineoplastic activity and safety between the four DPNAs at a low dose.

To further investigate differences in the safety among DPNAs, we investigated the acute toxicity of Taxotere and DPNAs in healthy BALB/c mice. The data of maximal tolerable dose (MTD), start lethal dose (SLD), and full lethal dose (FLD) in the test of acute toxicity were recorded in Supporting Information Table S8. Among them, the values of MTD of C₁₆-SS-DTX NPs (300 mg/kg), C₁₈-SS-DTX NPs (400 mg/kg), C₂₀-SS-DTX NPs (400 mg/kg), and C₂₄-SS-DTX NPs (500 mg/kg) were 6 times, 8 times, 8 times, and 10 times higher than Taxotere (50 mg/kg), respectively; the values of SLD of C₁₆-SS-DTX NPs (400 mg/kg), C₁₈-SS-DTX NPs (500 mg/kg), C₂₀-SS-DTX NPs (500 mg/kg), and C₂₄-SS-DTX NPs (600 mg/kg) were respectively 6.7 times, 8.3 times, 8.3 times, and 10 times higher than Taxotere (60 mg/kg); and the values of FLD of C₁₆-SS-DTX NPs (500 mg/kg), C₁₈-SS-DTX NPs (500 mg/kg), C₂₀-SS-DTX NPs

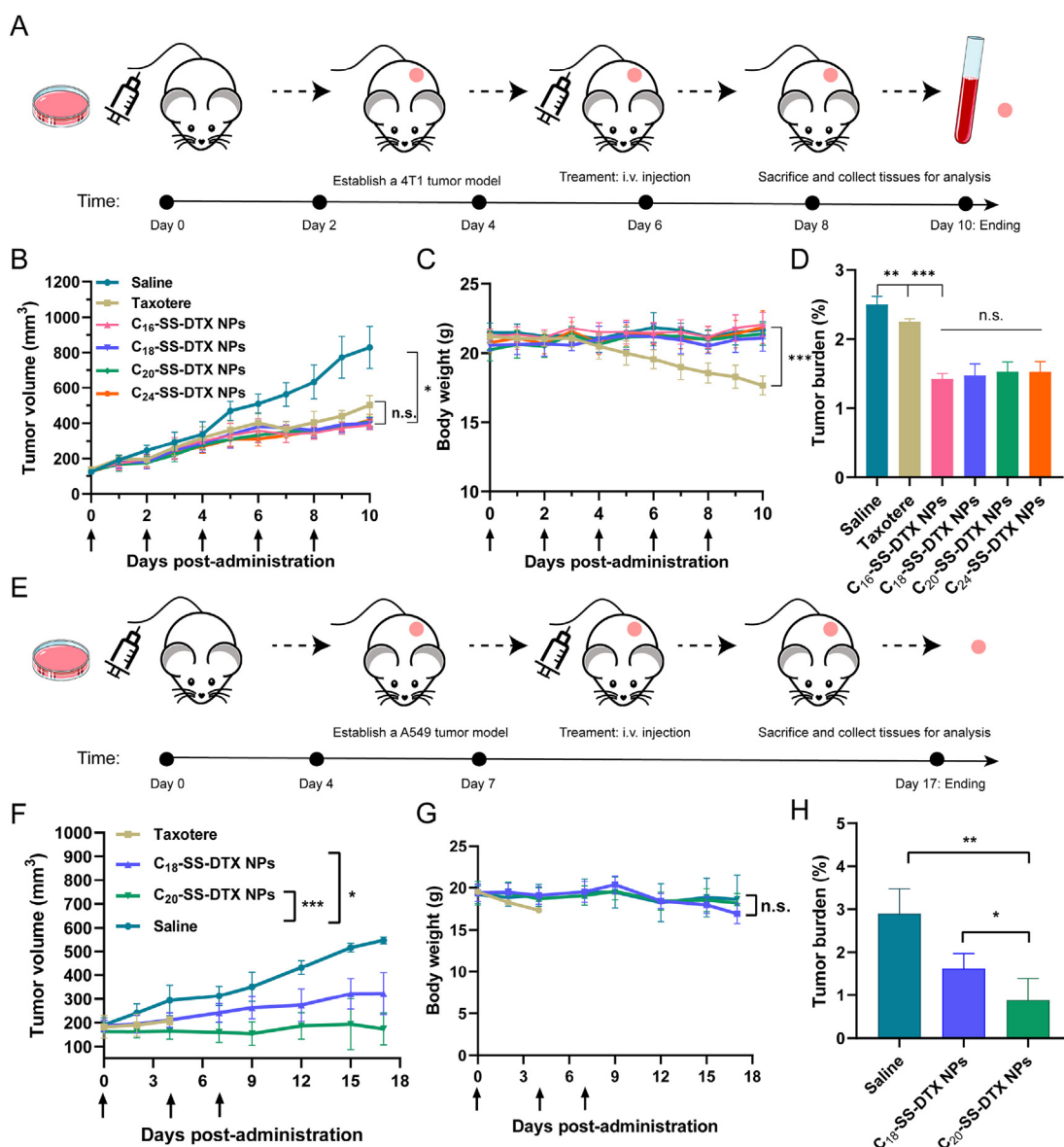


Figure 6 Antiproliferative activities of DPNAs. (A) Illustration of the experimental route of antiproliferative activities at 2.5 mg/kg. (B–D) Tumor growth profiles, body weight, and tumor burden at 2.5 mg/kg. Data are presented as mean \pm SD ($n = 5$). (E) Illustration of the experimental route of antiproliferative activities at 20 mg/kg. (F–H) Tumor growth profiles, body weight, and tumor burden at 20 mg/kg. Data are presented as mean \pm SD ($n = 3$). n.s. (no significance) $P > 0.05$, * $P < 0.05$, ** $P < 0.01$, *** $P < 0.001$, and **** $P < 0.0001$ by two-tailed Student's t -test.

(700 mg/kg), and C₂₄-SS-DTX NPs (700 mg/kg) were respectively 8.3 times, 8.3 times, 11.7 times, and 11.7 times higher than Taxotere (60 mg/kg). The slow-release rate of DTX from DPNAs in blood circulation reduced the exposure of DTX in normal tissues and organs, and significantly improved the safety and tolerated dose of DPNAs. Because C₁₆-SS-DTX NPs had the lowest stability and the highest release rate of DTX *in vivo*, C₁₆-SS-DTX NPs had the strongest acute toxicity among all DPNAs, while C₂₀-SS-DTX NPs and C₂₄-SS-DTX NPs had higher tolerance.

DPNAs with relatively high AUC values might pose cumulative toxicity risks. Thus, we studied the cumulative toxicity of Taxotere, C₂₀-SS-DTX NPs, and C₂₄-SS-DTX NPs in healthy BALB/c mice. The changes in body weight and the survival curve were shown in Supporting Information Fig. S15. All mice died after being treated with Taxotere at two different doses (30 and 45 mg/kg) three times. This indicated that the DPNAs exhibited higher safety than the Taxotere. Mice treated with C₂₀-SS-DTX NPs (30 and 45 mg/kg) and C₂₄-SS-DTX NPs (30 mg/kg) survived, while death occurred in those treated with C₂₄-SS-DTX NPs (45 mg/kg). And at the dose of 30 mg/kg, there was a significant difference in body weight between the two nanoassemblies. The results showed that the safety of C₂₄-SS-DTX NPs was poorer than that of C₂₀-SS-DTX NPs in the cumulative toxicity study. We believe there are two reasons for this: On the one hand, C₂₄-SS-DTX has a very high AUC value (the best pharmacokinetic parameter); On the other hand, it is reported that for long-chain fatty alcohols, the longer the carbon chain, the stronger the toxicity³⁴. This is caused by the production of more reactive oxygen species during the oxidation process of lipids with long carbon chains³⁵. It has been reported that lipids with long carbon chains are almost entirely metabolized by beta-oxidation in peroxisomes. Acyl-CoA oxidase 1 (ACOX1) is the rate-limiting step of peroxisome β -oxidation, which produces H₂O₂ during the desaturation of acyl-CoA to 2-*trans*-enolylase A³⁶. The above reasons lead to C₂₀-SS-DTX NPs showing better safety than C₂₄-SS-DTX NPs.

Therefore, we selected C₁₈-SS-DTX NPs and C₂₀-SS-DTX NPs with relatively good safety for further investigation of the antineoplastic activity in the A549 tumor model at high doses (20 mg/kg). The results (Fig. 6F–H) showed that all mice treated with Taxotere were dead on Day 7, while the mice in DPNAs groups survived at least until the end of the experiment (Day 17). It was proved that DPNAs had comparable antineoplastic and significantly higher safety compared with Taxotere. For DPNAs, C₂₀-SS-DTX NPs showed stronger antineoplastic activity than C₁₈-SS-DTX NPs. Meanwhile, there were no significant changes in body weight between C₂₀-SS-DTX NPs and saline after treatment. We analyzed that C₂₀-SS-DTX NPs could be accumulated more in the tumor due to the stable systemic circulation, thereby ensuring efficacy and reducing adverse events. In general, the shorter the carbon chains of the assembly modules corresponding, the faster the release efficiency, the stronger the cytotoxicity, and the stronger antineoplastic activity. However, too short length of carbon chains would lead to poor stability in the system and high toxicity. With the extension of the carbon chains of the assembly modules, the assembly ability and pharmacokinetic behavior of the prodrugs were improved, but too long carbon chains would also lead to cumulative toxicity risk. Compared to other DPNAs, the prodrug with 2-octyldecylalcohol as the assembly modules (C₂₀-SS-DTX) had the ideal balance between efficiency and safety.

Chemotherapy-related toxicity has always been a key problem that restricts clinical dosage and therapeutic effect. In this study, branched fatty alcohols with high self-assembly ability were used as the assembly modules of prodrugs to prepare DPNAs. Compared with Taxotere, the safety and dose tolerance of the prodrug nanoassemblies have been significantly improved, which demonstrated the advantages of branched fatty alcohols as assembly modules. On this basis, we further adjusted the safety of treatment by changing the length of the assembly modules. These works will provide a reference for the future clinical transformation of prodrug nanoassemblies.

4. Conclusions

Prodrug nanoassemblies with high drug loading and low carrier-related toxicity are a promising nanoplatform. However, keeping the balance between efficacy and safety by selecting suitable modules remains a great challenge for the development of prodrug nanoassemblies. The advantages of branched-chain fatty alcohols as assembly modules for prodrugs have been proposed in previous literature reports, but the effects of their properties on drug design have not been studied in detail²⁸. In this study, four prodrugs were designed using α -disulfide bonds as activation modules and different lengths of branched-chain fatty alcohols as assembly modules. As expected, all four prodrugs were able to form nanoassemblies with uniform particle sizes and high drug loading. Interestingly, differences between the lengths of assembly modules profoundly influenced the self-assembly stability, redox dual-sensitive drug release, cytotoxicity, pharmacokinetic properties, and antineoplastic activity of the DPNAs. The longer the carbon chain lengths of branched-chain fatty alcohols are, the stronger the self-assembly ability of prodrugs and the weaker the redox sensitivity are. However, more than expected, the carbon chain length of branched fatty alcohols is not linearly related to the safety of DPNAs. Considering the results of acute toxicity and cumulative toxicity, C₁₈-SS-DTX NPs and C₂₀-SS-DTX NPs have better safety due to relatively moderate redox sensitivity and assembly stability. With further research, we found that: the C₂₀-SS-DTX with the optimal combination of self-assembly stability and redox hypersensitivity ensured the ideal balance between efficacy and safety. This research has great reference significance for the rational design of prodrug nanoassemblies.

Acknowledgments

This work was financially supported by National Key R&D Program of China (No. 2022YFE0111600), National Natural Science Foundation of China (No. 82272151 and 82204318), Doctoral Scientific Research Staring Foundation of Liaoning Province (No. 2021-BS-130, China), General Program of Department of Education of Liaoning Province (No. LJKZ0953, China), Shenyang Young and Middle-aged Science and Technology Innovation Talents Support Program (RC220389, China).

Author contributions

Yinglei Zhai, Bingjun Sun, and Jin Sun designed and supervised this work. Shuo Wang and Tian Liu carried out the experiments and wrote the manuscript. Yuetong Huang, Chaoying Du, Danping Wang, and Xiyan Wang analyzed a part of the data. All authors have read and approved the final version of the manuscript.

Conflicts of interest

The authors have no conflicts of interest to declare.

Appendix A. Supporting information

Supporting data to this article can be found online at <https://doi.org/10.1016/j.apsb.2023.09.017>.

References

- Das T, Anand U, Pandey SK, Ashby Jr CR, Assaraf YG, Chen ZS, et al. Therapeutic strategies to overcome taxane resistance in cancer. *Drug Resist Updates* 2021;**55**:100754.
- Garon EB, Ciuleanu TE, Arrieta O, Prabhaskar K, Syrigos KN, Goksel T, et al. Ramucirumab plus docetaxel versus placebo plus docetaxel for second-line treatment of stage IV non-small-cell lung cancer after disease progression on platinum-based therapy (REVEL): a multicentre, double-blind, randomised phase 3 trial. *Lancet* 2014;**384**:665–73.
- Hellmann MD, Li BT, Chaft JE, Kris MG. Chemotherapy remains an essential element of personalized care for persons with lung cancers. *Ann Oncol* 2016;**27**:1829–35.
- Smith RA, Andrews KS, Brooks D, Fedewa SA, Manassaram-Baptiste D, Saslow D, et al. Cancer screening in the United States, 2019: a review of current American Cancer Society guidelines and current issues in cancer screening. *CA A Cancer J Clin* 2019;**69**:184–210.
- Li G, Jin Q, Xia F, Fu S, Zhang X, Xiao H, et al. Smart stimuli-responsive carrier-free nanoassembly of SN38 prodrug as efficient chemotherapeutic nanomedicine. *Acta Materia Medica* 2023;**2**:54–63.
- Li D, Wang Y, Li C, Wang Q, Sun B, Zhang H, et al. Cancer-specific calcium nanoregulator suppressing the generation and circulation of circulating tumor cell clusters for enhanced anti-metastasis combinational chemotherapy. *Acta Pharm Sin B* 2021;**11**:3262–71.
- Liu S, Khan AR, Yang X, Dong B, Ji J, Zhai G. The reversal of chemotherapy-induced multidrug resistance by nanomedicine for cancer therapy. *J Control Release* 2021;**335**:1–20.
- Wu W, Pu Y, Shi J. Nanomedicine-enabled chemotherapy-based synergistic cancer treatments. *J Nanobiotechnol* 2022;**20**:4.
- Sreekanth V, Kar A, Kumar S, Pal S, Yadav P, Sharma Y, et al. Bile acid tethered docetaxel-based nanomicelles mitigate tumor progression through epigenetic changes. *Angew Chem Int Ed Engl* 2021;**60**:5394–9.
- Li L, Zuo S, Dong F, Liu T, Gao Y, Yang Y, et al. Small changes in the length of diselenide bond-containing linkages exert great influences on the antitumor activity of docetaxel homodimeric prodrug nanoassemblies. *Asian J Pharm Sci* 2021;**16**:337–49.
- Sun B, Chen Y, Yu H, Wang C, Zhang X, Zhao H, et al. Photodynamic PEG-coated ROS-sensitive prodrug nanoassemblies for core-shell synergistic chemo-photodynamic therapy. *Acta Biomater* 2019;**92**:219–28.
- Sun B, Luo C, Cui W, Sun J, He Z. Chemotherapy agent-unsaturated fatty acid prodrugs and prodrug-nanoplatforms for cancer chemotherapy. *J Control Release* 2017;**264**:145–59.
- Sun B, Luo C, Zhang X, Guo M, Sun M, Yu H, et al. Probing the impact of sulfur/selenium/carbon linkages on prodrug nanoassemblies for cancer therapy. *Nat Commun* 2019;**10**:3211.
- Li G, Sun B, Li Y, Luo C, He Z, Sun J. Small-molecule prodrug nanoassemblies: an emerging nanoplatform for anticancer drug delivery. *Small* 2021;**17**:e2101460.
- Liu T, Li L, Wang S, Dong F, Zuo S, Song J, et al. Hybrid chalcogen bonds in prodrug nanoassemblies provides dual redox-responsivity in the tumor microenvironment. *Nat Commun* 2022;**13**:7228.
- Zhang M, Gao S, Yang D, Fang Y, Lin X, Jin X, et al. Influencing factors and strategies of enhancing nanoparticles into tumors *in vivo*. *Acta Pharm Sin B* 2021;**11**:2265–85.
- Zhang Y, Li M, Gao X, Chen Y, Liu T. Nanotechnology in cancer diagnosis: progress, challenges and opportunities. *J Hematol Oncol* 2019;**12**:137.
- Hu C, He X, Chen Y, Yang X, Qin L, Lei T, et al. Metformin mediated PD-L1 downregulation in combination with photodynamic-immunotherapy for treatment of breast cancer. *Adv Funct Mater* 2021;**31**:2007149.
- Liu R, Luo C, Pang Z, Zhang J, Ruan S, Wu M, et al. Advances of nanoparticles as drug delivery systems for disease diagnosis and treatment. *Chin Chem Lett* 2023;**34**:107518.
- Li Y, Lin J, Wang P, Luo Q, Zhu F, Zhang Y, et al. Tumor microenvironment cascade-responsive nanodrug with self-targeting activation and ROS regeneration for synergistic oxidation-chemotherapy. *Nano-Micro Lett* 2020;**12**:182.
- Hong S, Lee Y, Shin H, Kim T, Jung E, Lee D. Nanoassemblies of disulfide-bridged bile acid dimers as therapeutics agents for hepatic ischemia/reperfusion injury. *ACS Appl Bio Mater* 2021;**4**:3145–54.
- Huang L, Chen X, Bian Q, Zhang F, Wu H, Wang H, et al. Photosensitizer-stabilized self-assembling nanoparticles potentiate chemo-photodynamic efficacy of patient-derived melanoma. *J Control Release* 2020;**328**:325–38.
- Jun H, Jeon C, Kim S, Song N, Jo H, Yang M, et al. Nanoassemblies of self-immolative boronate-bridged retinoic acid dimeric prodrug as a clot-targeted self-deliverable antithrombotic nanomedicine. *ACS Nano* 2023;**17**:12336–46.
- Yang K, Yu G, Yang Z, Yue L, Zhang X, Sun C, et al. Supramolecular polymerization-induced nanoassemblies for self-augmented cascade chemotherapy and chemodynamic therapy of tumor. *Angew Chem Int Ed Engl* 2021;**60**:17570–8.
- Yang Y, Sun B, Zuo S, Li X, Zhou S, Li L, et al. Trisulfide bond-mediated doxorubicin dimeric prodrug nanoassemblies with high drug loading, high self-assembly stability, and high tumor selectivity. *Sci Adv* 2020;**6**:eabc1725.
- Fattahi N, Shahbazi MA, Maleki A, Hamidi M, Ramazani A, Santos HA. Emerging insights on drug delivery by fatty acid mediated synthesis of lipophilic prodrugs as novel nanomedicines. *J Control Release* 2020;**326**:556–98.
- Zhang C, Jin S, Xue X, Zhang T, Jiang Y, Wang PC, et al. Tunable self-assembly of Irinotecan-fatty acid prodrugs with increased cytotoxicity to cancer cells. *J Mater Chem B* 2016;**4**:3286–91.
- Wang D, Du C, Wang S, Li L, Liu T, Song J, et al. Probing the role of connecting bonds and modifying chains in the rational design of prodrug nanoassemblies. *ACS Appl Mater Interfaces* 2022;**14**:51200–11.
- Wang X, Li L, Wang D, Zuo S, Liu T, Dong F, et al. Minor change in the length of carbon chain has a great influence on the antitumor effect of paclitaxel-fatty alcohol prodrug nanoassemblies: small roles, big impacts. *Nano Res* 2021;**15**:3367–75.
- Sun B, Luo C, Yu H, Zhang X, Chen Q, Yang W, et al. Disulfide bond-driven oxidation- and reduction-responsive prodrug nanoassemblies for cancer therapy. *Nano Lett* 2018;**18**:3643–50.
- Zuo S, Sun B, Yang Y, Zhou S, Zhang Y, Guo M, et al. Probing the superiority of diselenium bond on docetaxel dimeric prodrug nanoassemblies: small roles taking big responsibilities. *Small* 2020;**16**:e2005039.
- Perez-Herrero E, Fernandez-Medarde A. Advanced targeted therapies in cancer: drug nanocarriers, the future of chemotherapy. *Eur J Pharm Biopharm* 2015;**93**:52–79.
- Yang Y, Zuo S, Zhang J, Liu T, Li X, Zhang H, et al. Prodrug nanoassemblies bridged by mono-/di-/tri-sulfide bonds: exploration is for going further. *Nano Today* 2022;**44**:101480.
- Liu L. Application of electrotopological state index for atom type to the study of aliphatic alcohol toxicity prediction. *Acta Chim Sin* 2008;**66**:1873–8.
- Maloney E, Sweet IR, Hockenbery DM, Pham M, Rizzo NO, Tateya S, et al. Activation of NF-kappaB by palmitate in endothelial cells: a key role for NADPH oxidase-derived superoxide in response to TLR4 activation. *Arterioscler Thromb Vasc Biol* 2009;**29**:1370–5.
- Ding L, Sun W, Balaz M, He A, Klug M, Wieland S, et al. Peroxisomal beta-oxidation acts as a sensor for intracellular fatty acids and regulates lipolysis. *Nat Metab* 2021;**3**:1648–61.